International Journal of Heat and Mass Transfer 51 (2008) 5088–5096

Contents lists available at ScienceDirect

International Journal of Heat and Mass Transfer

journal homepage: www.elsevier.com/locate/ijhmt

Three-dimensional laminar slip-flow and heat transfer in a rectangular microchannel with constant wall temperature

H.D. Madhawa Hettiarachchi, Mihajlo Golubovic, William M. Worek *, W.J. Minkowycz

Department of Mechanical and Industrial Engineering, University of Illinois at Chicago, 842 W Taylor Street, Chicago, IL 60607, United States

ARTICLE INFO

Article history:
Received 19 November 2007
Revised in revised form 21 February 2008
Available online 10 May 2008

Keywords:
Microchannel
Slip-flow
Heat transfer
Knudsen number
Rarefaction
Simultaneously developing

ABSTRACT

Three-dimensional laminar slip-flow and heat transfer in rectangular microchannels having constant temperature walls are studied numerically using the finite-volume method for thermally and simultaneously developing flows. The Navier–Stokes and energy equations are solved with velocity slip and temperature jump at the wall. A modified convection–diffusion coefficient at the wall–fluid interface is defined to incorporate the temperature-jump boundary condition. Validity of the numerical simulation procedure is established and the effect of rarefaction on hydrodynamicaly developing flow field, pressure gradient and entrance length is analyzed. A correlation for the fully developed friction factor is presented as a function of Knudsen number (Kn) and aspect ratio (α). The influence of rarefaction on the Nusselt (Nu) number is investigated for thermally and simultaneously developing flows. The effect of velocity slip is found to increase the Nu number, while the temperature-jump tends to decrease it, and the combined effect could result in an increase or a decrease in the Nu number. In the fully developed region, there could be high as 15% increase or low as 50% decrease in Nu number is plausible for the range of parameters considered in this work.

1. Introduction

Conventional examples of fluids in slip-flow conditions include low pressure fluidic flow systems such as those occurring in vacuum and aerospace engineering devices [1]. Recent advances in micro–nano fabrication technologies and development of microscale thermal fluidic systems have opened a new area where the dynamics of slip-flow is applicable [2].

One of the major difficulties predicting the flow of fluids in micro- and nano-sized channels can be attributed to the rarefaction effects that occur in the fluids when the channel dimensions become comparable to the mean free path of the fluid molecules. These circumstances result in non-continuum regions in the fluid that will influence the velocity profile, pressure drop and heat transfer in the channels. Knudsen number is a measure of the degree of the rarefaction which is defined as the ratio of mean free path to the characteristic length scale of the system. For small Knudsen numbers, $Kn \leqslant 10^{-3}$, the fluid is considered to be a continuum, while for large values, $Kn \geqslant 10$, free molecular flow is assumed. The slip-flow region studied in this paper has Knudsen number in the range of $10^{-3} \leqslant Kn \leqslant 10^{-1}$, where molecular collisions with the walls dominate over intermolecular collisions resulting in a breakdown of the continuum assumption in a thin region adjacent to the walls.

It is well established that for the slip-flow regime, the standard Navier–Stokes equations can still be used with modified boundary conditions for slip velocity at the walls. Previous experimental, numerical and analytical studies on gaseous flows in microchannels [3–11] strongly support the applicability of the continuum approach in combination with velocity slip boundary condition to solve the slip-flow problems in microscale fluidic systems. Primarily, the effect of rarefaction on the velocity profile and pressure distribution was analyzed and most of the numerical and analytical studies were performed in a two-dimensional coordinate system often with simplified assumptions to the governing equations. Dongari et al. [12] and Choi et al. [13] have analyzed different slip-flow models and their validity for range of Knudsen numbers.

Slip-flow heat transfer in parallel plate microchannels have been studied by numerous authors [14–17] for different boundary conditions. Hadjiconstantinou and Simek [17] showed that for the slip-flow region, the continuum approach prediction is in good agreement with the direct simulation Monte Carlo (DSMC) results. The extended Graetz problem with velocity slip and temperature jump at the wall has been studied analytically and numerically for the cases of constant wall temperature and constant heat flux boundary conditions by several researchers [18–23]. Axial conduction effects were neglected in all solutions and the simplified energy equation was solved assuming hydrodynamically fully

* Corresponding author. Tel.: +1 312 996 5610; fax: +1 312 413 0447.
E-mail address: wworek@uic.edu (W.M. Worek).

0017-9310/$ - see front matter © 2008 Elsevier Ltd. All rights reserved.
doi:10.1016/j.ijheatmasstransfer.2008.02.049

Nomenclature

a	convection–diffusion parameter
A	area
c_p	specific heat
D_h	hydraulic diameter
Ec	Eckert number
fRe	friction relation
H	non-dimensionalized height of microchannel
k	thermal conductivity
Kn	Knudsen number
L	non-dimensionalized length of microchannel
Nu	Nusselt number
p	pressure
P	non-dimensionalized pressure
P^*	guessed pressure
P'	pressure correction
Pe	Peclet number
Pr	Prandtl number
Re	Reynolds number
T	temperature
u	fluid velocity
U	non-dimensional fluid velocity
W	non-dimensionalized width of microchannel
X, Y, Z	non-dimensional coordinates
Z^+	non-dimensional axial length, $Z/(D_hRe)$
Z^*	reciprocal Graetz number, $Z/(D_hPrRe)$

Greek symbols

α	aspect ratio
β	parameter defined by Eq. (10)
γ	specific heat ratio
θ	non-dimensionalized temperature
μ	viscosity
ρ	density
σ_T	thermal accommodation coefficient
σ_V	momentum accommodation coefficient
ϕ	eigen values defined by Eq. (13)
φ	independent variable

Subscripts

ave	average
i, j, k	array indices
in	inlet
wall	wall surface
N, S, E, W, T, B	neighboring grid points

developed velocity profile. Slip-flow heat transfer in rectangular microchannels has been studied by several researches [24–29]. Yu and Ameel [24,25] studied laminar slip-flow forced convection under thermally developing flow for constant wall temperature and isoflux boundary conditions. The energy equation was solved analytically using integral transform technique neglecting axial conduction and the heat transfer augmentation due to rarefaction was studied. Renksizbulut et al. [26] solved slip-flow and heat transfer in the entrance region of rectangular microchannels for cases where Prandtl number is equal to unity.

In slip-flow region, it was assumed that the temperature of the fluid adjacent to the wall was finitely different from the wall surface temperature due to breakdown of the continuum flow near the walls. The above studies show the importance of implementing the temperature jump boundary condition in solving energy equation in the slip-flow region and neglecting it could lead to a significant over prediction of the heat transfer.

The entrance region in a microchannel is particularly of interest due to the presence of large pressure drop and heat transfer, and the relative size. Also, the effect of axial conduction becomes important for low Peclet numbers ($Pe = RePr$) which is typical in microchannel flows. In this study, three-dimensional slip-flow and heat transfer in rectangular microchannels are investigated for thermally and simultaneously developing flows and axial conduction effect is included in the solution. The non-dimensionalized governing equations are solved using the SIMPLE finite-volume method. Implementation of the temperature-jump and discretization of the energy equation at the fluid wall interface is explained. The effect of rarefaction on hydrodynamically developing flow field and pressure gradient in the entrance region is analyzed. Variation of the entrance length with Kn is investigated for different aspect ratios. A correlation for the fully developed fRe is presented as a function of Kn and aspect ratio. The influence of Peclet number and rarefaction on the Nusselt number is studied in detail for thermally and simultaneously developing flows.

2. Analysis

The schematic of the microchannel and coordinate system considered in this analysis are shown in Fig. 1. The aspect ratio is given by $\alpha = H/W$, where H and W are the dimensionless height and width of the channel. The flow is considered along the Z-axis and the channel length is chosen so that hydrodynamically and thermally developed flow is reached at the exit. A constant temperature boundary condition is assumed at the outer wall surfaces.

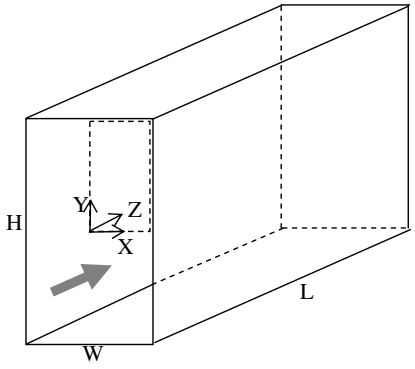

Fig. 1. Schematic diagram of the rectangular microchannel passage.

The numerical model for fluid flow and heat transfer in the microchannel was developed under the following assumptions:

- Steady fluid flow and heat transfer.
- The flow is incompressible and laminar.
- Constant fluid properties.
- Negligible radiation heat transfer.
- Body forces and viscous dissipation are ignored.
- Rarefaction effects set velocity slip and temperature-jump at the fluid–wall interface.

Based on the above assumptions, the governing equations describing fluid flow and heat transfer in the microchannel can be written as follows:

The momentum equation,

$$\rho u_j \frac{\partial u_i}{\partial x_j} = \mu \nabla^2 u_i + \frac{\partial p}{\partial x_i}, \tag{1}$$

and the energy equation

$$\rho c_p u_j \frac{\partial T_i}{\partial x_j} = k\nabla^2 T. \tag{2}$$

The momentum and energy equations are non-dimensionalized using following dimensionless parameters:

$$X_i = \frac{x_i}{D_h}, \quad U_i = \frac{u_i}{u_{ave}}, \quad P = \frac{p}{\rho u_{ave}^2} \quad \text{and} \quad \theta = \frac{T - T_{in}}{T_{wall} - T_{in}}. \tag{3}$$

The non-dimensionalized momentum equation becomes

$$U_j \frac{\partial U_i}{\partial X_j} = \frac{1}{Re}\nabla^2 U_i + \frac{\partial P}{\partial X_i}, \tag{4}$$

and the non-dimensionalized energy equation is

$$U_j \frac{\partial \theta}{\partial X_j} = \frac{1}{RePr}\nabla^2 \theta. \tag{5}$$

At the channel inlet, two different fluid velocity profiles are assumed; uniform and fully developed. In addition, a uniform temperature profile ($\theta_{in} = 0$) is prescribed. At the exit, since the fully developed conditions are assumed, the Z direction velocity and temperature gradients are set to zero. A zero pressure is assigned at the flow exit while zero pressure gradient is applied to all other boundaries including the inlet. A constant wall temperature ($\theta_{wall} = 1$) is maintained at the wall while the fluid flow satisfies velocity jump and temperature jump at the walls.

2.1. Slip velocity and temperature jump boundary conditions

In a traditional (i.e., continuum) flow analysis, velocity and temperature continuity is enforced along all fluid–wall interfaces. In the no-slip-flow region, a discontinuity of the velocity and temperature at the fluid–wall interface arises due to breakdown of the local thermodynamic equilibrium between the wall and the adjacent fluid. The velocity slip and temperature jump of the fluid adjacent to the wall is proportional to normal velocity and temperature gradients at the fluid–wall interface.

The non-dimensionalized tangential velocity slip at the fluid–wall interface is expressed as [2]

$$U = \left(\frac{2 - \sigma_V}{\sigma_V}\right) Kn \frac{\partial U}{\partial n} + \frac{3}{2\pi}\frac{(\gamma - 1)}{\gamma}\frac{Kn^2 Re}{Ec}\frac{\partial \theta}{\partial Z}. \tag{6}$$

$\frac{\partial U}{\partial n}$ is the transverse velocity gradient and $\frac{\partial \theta}{\partial Z}$ is the tangential temperature gradient in the fluid at the fluid–wall interface. The first term of Eq. (6) represents the slip-flow induced by the transverse velocity gradient, while the second term accounts the slip-flow induced by the thermal creep. The second term becomes negligible since $\partial/\partial n \gg \partial/\partial Z$ at the wall for moderate temperature gradient slip-flows and also due to fact that it is second order in Knudsen number.

Similarly, the non-dimensionalized temperature jump at the fluid–wall interface is given by [2]

$$\theta - \theta_{wall} = \frac{2 - \sigma_T}{\sigma_T}\left(\frac{2\gamma}{\gamma + 1}\right)\frac{Kn}{Pr}\frac{\partial \theta}{\partial n}. \tag{7}$$

$\frac{\partial \theta}{\partial n}$ is the transverse temperature gradient in the fluid at the fluid–wall interface. The tangential momentum accommodation coefficient, σ_V, and thermal accommodation coefficient, σ_T, describe the interaction of the fluid molecules with the wall. Generally the values of these coefficients depend on the surface finish, temperature and velocity at the fluid–wall interface, and are determined experimentally. It varies from near zero to unity for specular and diffuse reflections, respectively. For most engineering applications, values of accommodation coefficients are near unity and considering approximate nature of the slip-flow they are taken as unity in this present study.

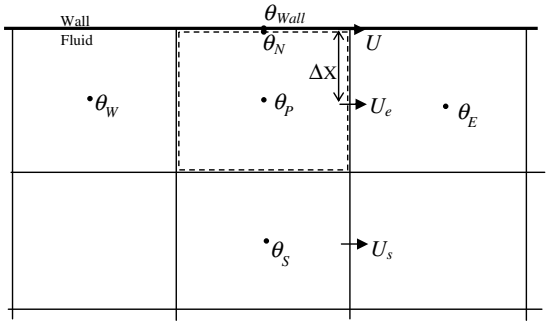

Fig. 2. Control volume adjacent to the wall (only two-dimensions are shown for the simplicity).

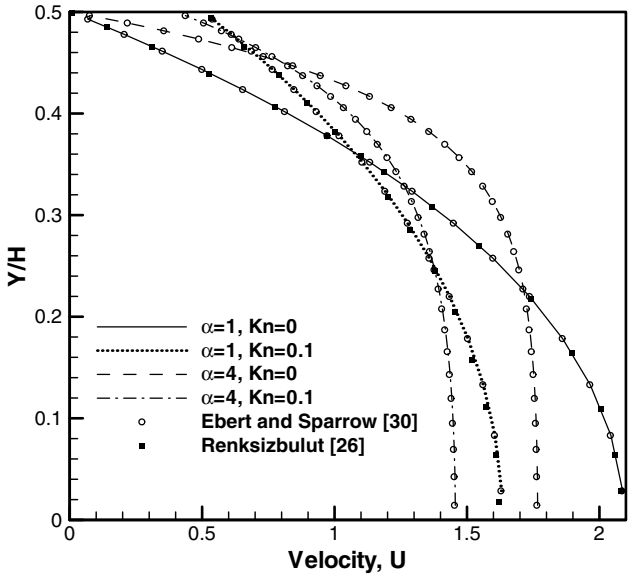

Fig. 3. Comparison of the fully developed velocity profile along the Y-axis ($X = 0$, $Z = 0$) with the results of Renksizbulut et al. [26] and Ebert and Sparrow [30].

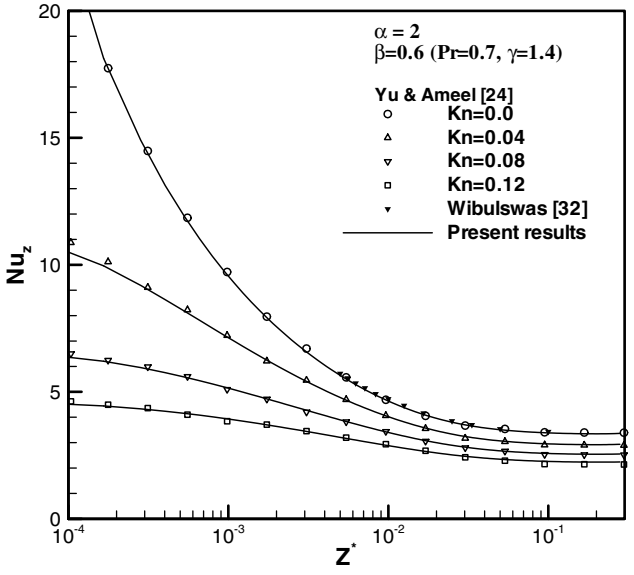

Fig. 4. Comparison of the local Nusselt number (assuming negligible axial conduction) along the microchannel axis with the results of Yu and Ameel [24] and Wibulswas [32].

The non-dimensional form of the simplified slip-flow velocity and temperature-jump boundary conditions can be expressed as

$$U = Kn\frac{\partial U}{\partial n}, \quad \text{and} \tag{8}$$

$$\theta - \theta_{\text{wall}} = \frac{Kn}{\beta}\frac{\partial \theta}{\partial n}, \tag{9}$$

$$\text{where} \quad \beta = \left(\frac{\gamma+1}{2\gamma}\right)Pr. \tag{10}$$

The parameter β is a function of Prandtl number, Pr, and specific heat ratio, γ.

Ebert and Sparrow [30] have presented an analytical equation for fully developed slip-flow velocity profile in a rectangular channel and it can be presented according to the coordinate system and non-dimensional parameters considered in this analysis as follows:

$$U(X,Y) = \frac{HW}{4A}\sum_{k=1}^{\infty}\frac{\cos\phi_k X}{\phi_k^3}\left(\frac{\sin(\phi_k H/2)}{(H/2+Kn\sin^2(\phi_k H/2))}\right) \times\left(1-\frac{\cosh\phi_k Y}{\cosh\phi_k W/2 + Kn\phi_k\sinh(\phi_k W/2)}\right), \tag{11}$$

where

$$A = \sum_{k=1}^{\infty}\phi_k^{-5}\left(\frac{\sin^2\phi_k H/2}{H/2+Kn\sin^2\phi_k H/2}\right) \times\left(\phi_k W/2 - \frac{\tanh\phi_k W/2}{1+Kn\phi_k\tanh\phi_k W/2}\right), \tag{12}$$

and values of ϕ_k are evaluated using the eigenfunction

$$\cot(\phi_k H/2) = \phi_k Kn. \tag{13}$$

3. Numerical solution

Due to symmetry, a quarter of the channel is considered in the analysis. A non-uniform grid arrangement is used in the X, Y and Z directions. A large number of grid points are used near the channel inlet and fluid–wall interface to resolve the developing flow region and large velocity and thermal gradients.

The numerical solution is obtained by discretizing the governing equations using the finite-volume method as described by

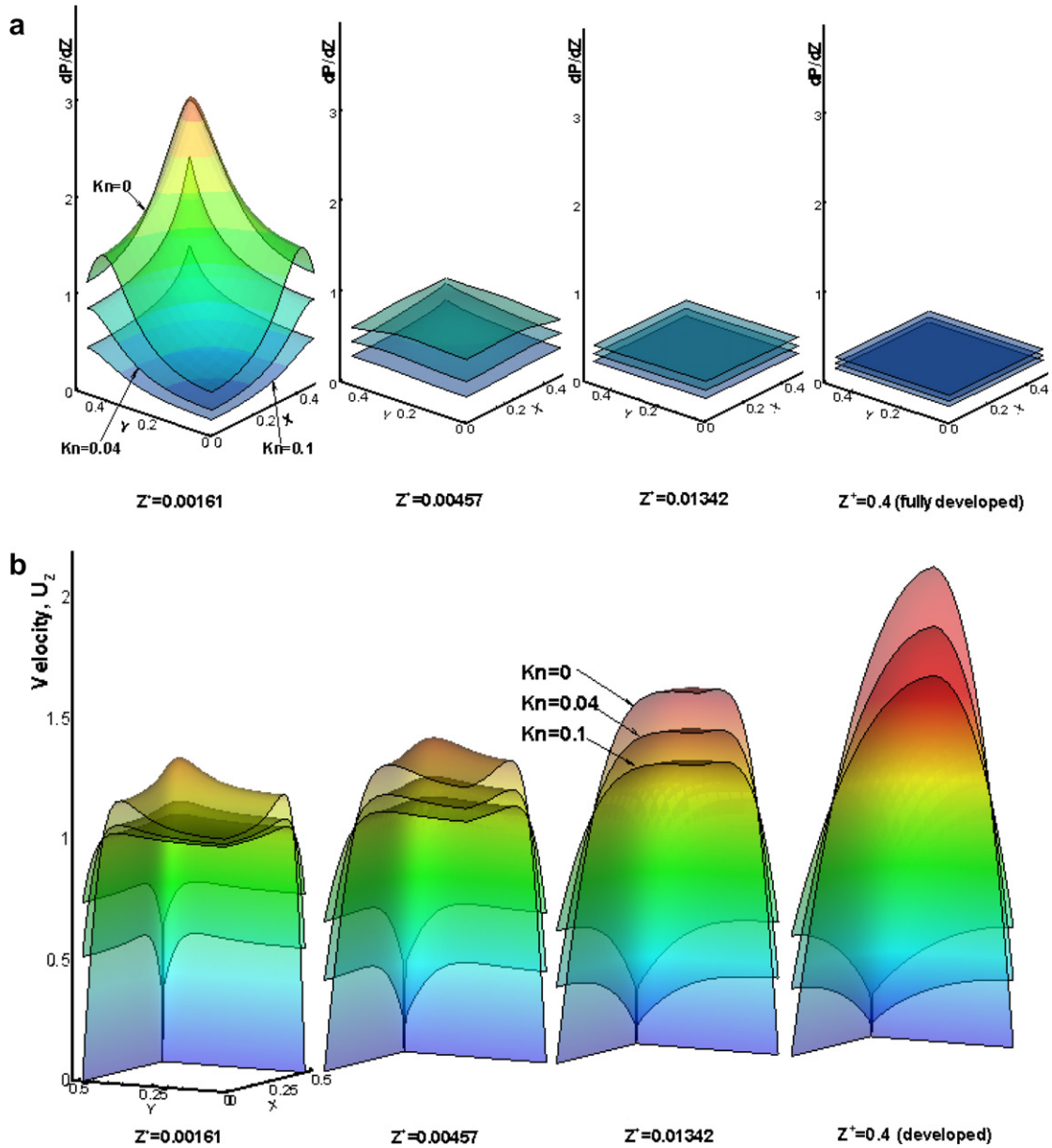

Fig. 5. Developing (a) pressure-gradient and (b) velocity profiles at different cross-sections along a square microchannel for $Re = 100$ and $Kn = 0$, 0.04 and 0.1.

Patankar [31]. A power law scheme is used to interpolate the convection–diffusion coefficients at the faces of control volumes. The pressure–velocity coupling is obtained using the Simple algorithm [31]. To enhance the convergence rate, the pressure field is updated with an additional pressure correction term based on the average velocity deviation at each cross-section as shown below

$$P = P^* + P' + \frac{(U_{ave,z=0} - U_{ave,z})}{Re}. \tag{14}$$

This procedure significantly improves the convergence rate of the solution. The resulting set of algebraic equations is solved using line-by-line method. The solution is assumed converged when $|(\phi^{n+1} - \phi^n)/\phi^{n+1}| \leqslant 10^{-6}$ is satisfied for all independent variables.

3.1. Implementation of the velocity slip and temperature jump boundary conditions

A control volume adjacent to the boundary is shown in Fig. 2. (For the simplicity a two-dimensional diagram is shown). A staggered-mesh arrangement is considered in this analysis. Slip velocity at the wall is given by Eq. (8). By using a first order approximation for the normal velocity gradient in Eq. (8), the slip velocity can be expressed as a function of the neighboring velocity, U_e, as

$$U = \left(\frac{Kn/\Delta X}{1 + Kn/\Delta X}\right) U_e, \tag{15}$$

which is then incorporated in to the numerical solution as a coupled boundary condition.

A discretized energy equation for a control volume adjacent to the wall can be written as [30]

$$a_N(\theta_N - \theta_P) + a_S(\theta_S - \theta_P) + a_E(\theta_E - \theta_P) + a_W(\theta_W - \theta_P) + a_T(\theta_T - \theta_P) + a_B(\theta_B - \theta_P) + b = 0, \tag{16}$$

where the coefficients a's present the convection and diffusion influence at the six faces of the boundary volume as shown in Fig. 2. (For simplicity only two-dimensions are shown). The terms θ_{wall} and θ_N are the temperatures at the wall and liquid–wall interface, respectively, which could be assumed infinitesimal distance apart.

The temperature jump at the fluid–wall interface can be written as

$$\theta_N - \theta_{wall} = \frac{Kn}{\beta}\frac{\partial\theta}{\partial n}. \tag{17}$$

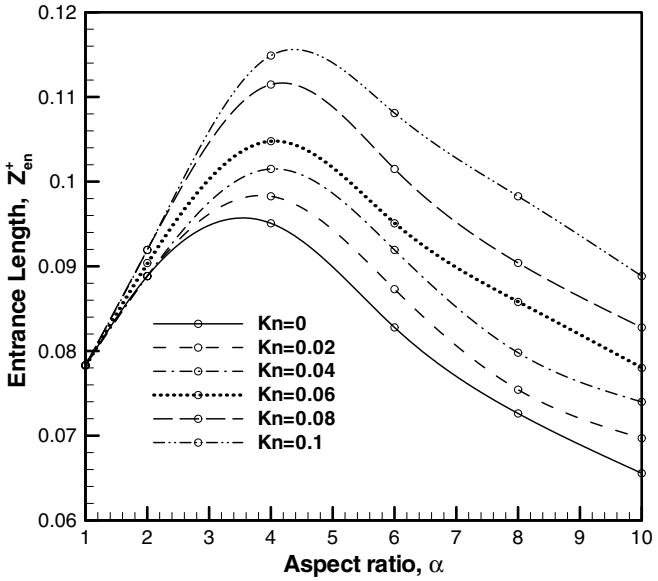

Fig. 6. Variation of entrance length with channel aspect ratio (α) at different Knudsen number (Kn) values.

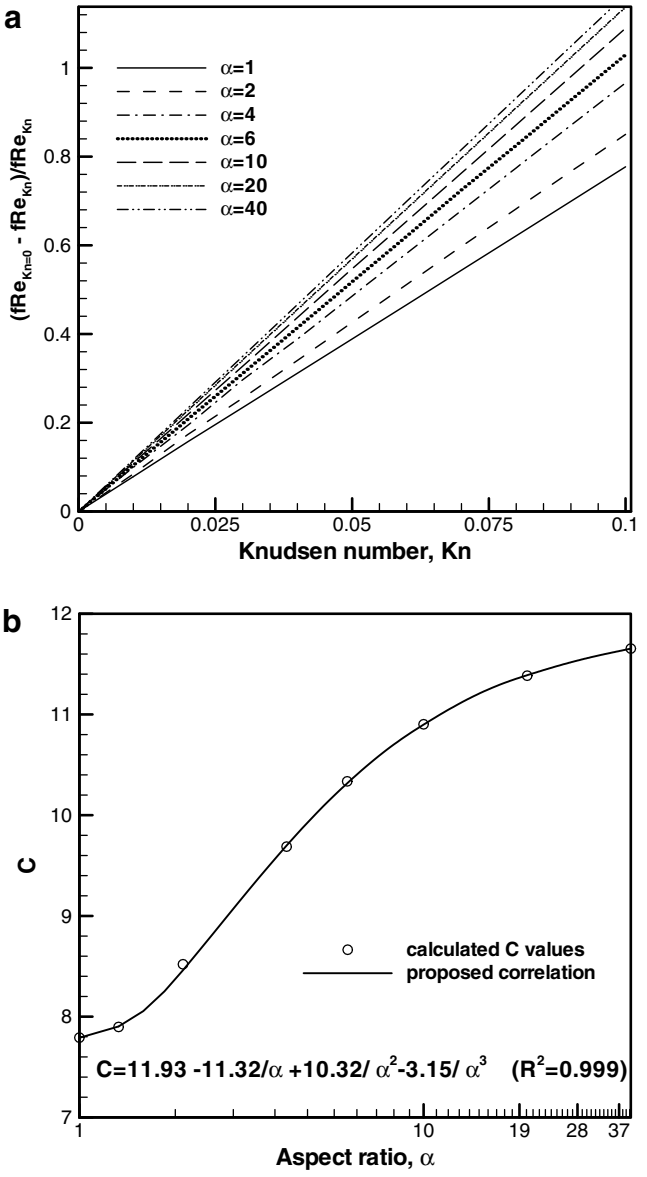

Fig. 7. Fully developed slip-flow friction relation as a function of Kn number and aspect ratio, α: (a) variation of $\left(\frac{(fRe)_{Kn=0}}{(fRe)_{Kn}} - 1\right)$ with Kn and α & (b) proposed correlation for C as a function of α.

Table 1
Comparison of fully developed fRe for laminar no slip-flow in rectangular channels with the results of Shah and London [33]

Aspect ratio, α	1	2	4	6	10	20	40
fRe, Shah and London [33]	14.227	15.548	18.233	19.702	21.169	22.477	23.215
fRe, Present calculation	14.219	15.485	18.145	19.571	21.023	22.315	23.069

By using a first order approximation for the normal temperature gradient, $\frac{\partial\theta}{\partial n} = \frac{(\theta_P - \theta_N)}{\Delta X}$, in Eq. (17) and rearranging, the term $(\theta_P - \theta_N)$ can be written as

$$\theta_P - \theta_N = \frac{(\theta_P - \theta_{wall})}{\left(1 + \frac{1}{\beta}\frac{Kn}{\Delta X}\right)}. \tag{18}$$

By substituting Eq. (18) into Eq. (15), the discretized energy equation can be expressed for a boundary control volume as

$$a_N^*(\theta_{wall} - \theta_P) + a_S(\theta_S - \theta_P) + a_E(\theta_E - \theta_P) + a_W(\theta_W - \theta_P) + a_T(\theta_T - \theta_P) + a_B(\theta_B - \theta_P) + b = 0, \tag{19}$$

where, a modified boundary convection–diffusion coefficient, a_N^*, can be defined as

$$a_N^* = \frac{a_N}{\left(1 + \frac{1}{\beta}\frac{Kn}{\Delta X}\right)}. \tag{20}$$

Thus, the discretized equations for boundary control volumes can be written similar to internal control volumes with a simple adjustment to the boundary convection–diffusion coefficient, a_N, as shown in Eq. (20).

3.2. Grid independence and validation

A non-uniform grid is considered in the *X*, *Y* and *Z* directions with a fine grid near the channel walls and at the entrance region where large gradients are exist. The grid independence of the results was carried out by using different mesh sizes, and it was found that any grid size beyond $16 \times 16 \times 200$ (with a stretching ratio of 4:4:100 in *X*, *Y* and *Z* directions, respectively) yields grid independent results for a square channel. For larger aspect ratios, the grid size was scaled accordingly to maintain the grid independence.

The numerical code is validated by comparing results with the available analytical and numerical results. Fig. 3 shows the fully developed velocity profile along the *Y*-axis at different aspect ratios and Knudsen numbers. Excellent agreement was found between the present numerical results and the published numerical [26] and analytical [30] data. The local *Nu* number along the microchannel axis is compared with the analytical solution presented by Yu and Ameel [24] for the case of thermally developing flow with uniform temperature boundary condition and negligible fluid axial conduction. Very good agreement was observed between the pres-

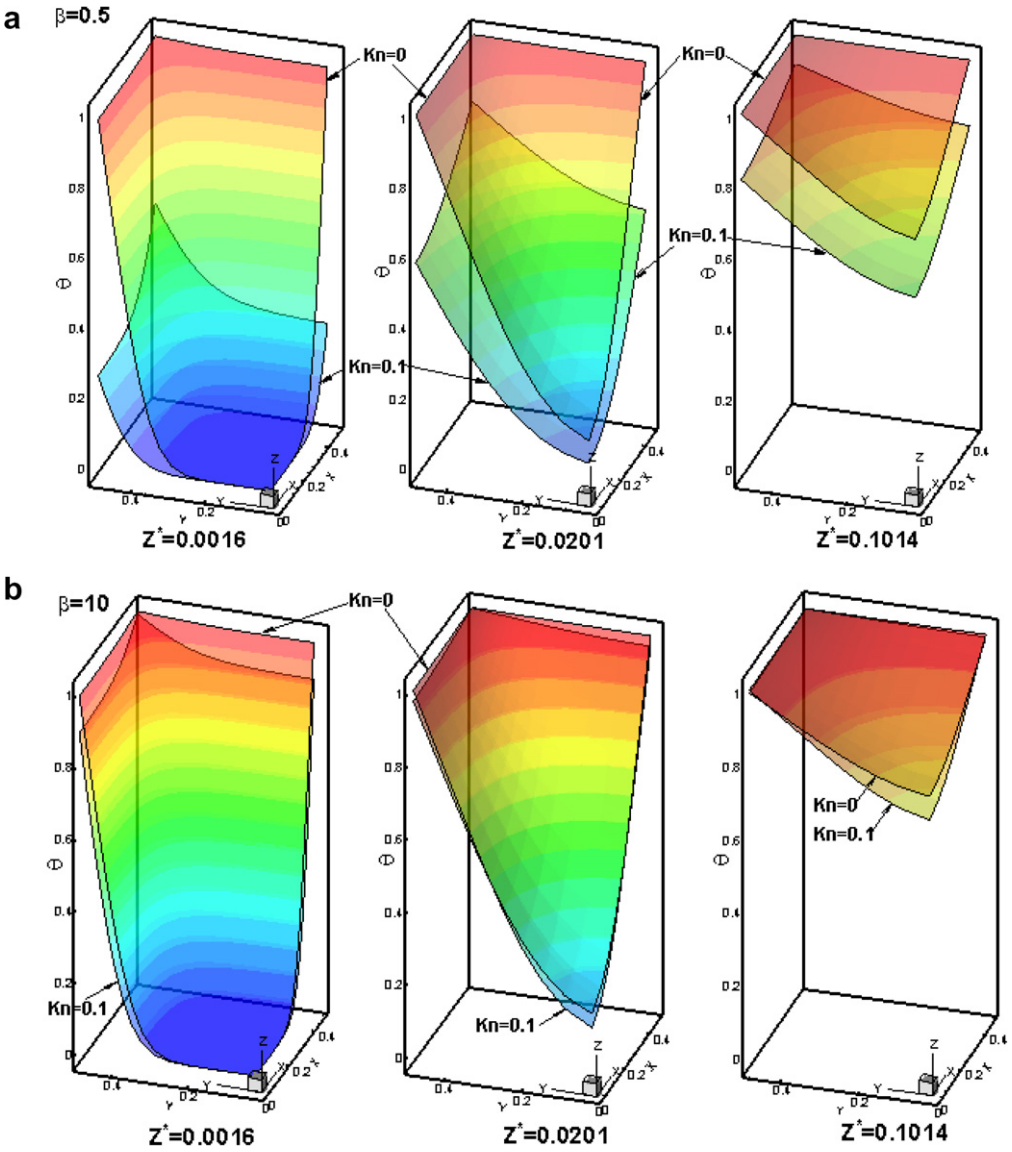

Fig. 8. Effect of rarefaction on the thermally developing temperature profile at different cross-sections along the length of a square microchannel for *Pe* = 100 and *Kn* = 0 and 0.1 at (a) $\beta = 0.5$ and (b) $\beta = 10$.

ent calculation and the Yu and Ameel [24] solution at different Knudsen numbers as shown in Fig. 4. Further, the present solution agrees well with the no-slip-flow data by Wilbulswas [32].

4. Results and discussion

Rarefaction effects on the fluid flow and heat transfer in the rectangular microchannels with constant wall temperature are examined using two-dimensionless parameters, Kn ($0 < Kn < 0.1$) and β ($0.5 < \beta < 10$), that include the effects of velocity slip and temperature jump.

4.1. Hydrodynamically developing flow field

Fig. 5 shows the effect of slip-flow on the developing pressure gradient and velocity profiles at different cross-sections in the entrance region for a square microchannel. The pressure gradient and velocity profiles for three different Knudsen numbers are shown. For no-slip-flow condition (i.e., $Kn = 0$), local pressure gradient and velocity maxima can be observed near the walls in the very beginning of the entrance region, particularly near the corner region. This is because of a sudden drop of fluid momentum adjacent to the walls due to the no slip boundary condition. As the slip increases (i.e., Knudsen number increases), the pressure gradient and the velocity maximums diminish since the velocity slip allows the fluid near the walls to keep part of its momentum. As the flow develops along the channel, the pressure gradient profiles become uniform across the cross-section and an increase in the Kn number results in lower pressure gradients as shown in Fig. 5a. At a given cross-section, the slip velocity varies along the periphery and reaches a minimum at the corners, and the maximum velocity which occurs in the core region decreases with increasing Kn number as shown in Fig. 5b.

4.2. Entrance length

Fig. 6 shows the variation of the entrance length with the channel aspect ratio at different Kn numbers. A uniform inlet velocity profile is assumed and the dimensionless entrance length, Z^+_{en}, is defined as the distance where the maximum velocity reaches 99% times the corresponding fully developed value. The entrance length increases as the aspect ratio increases until it reaches a maximum near an aspect ratio of four and then it decreases as the aspect ratio increases further. As the aspect ratio increases and the channel becomes more flat, the influence of the shorter side walls and corner regions on the core velocity diminishes resulting in a decrease in the entrance length. The Knudsen number has an increasing effect on the entrance length for all aspect ratios except for the aspect ratios near unity where negligible increase was observed as shown in Fig. 6.

4.3. Fully developed friction relation fRe

The friction relation, fRe, calculated for the fully developed no-slip-flow at different aspect ratios is in good agreement with the data given by Shah and London [33] as shown in Table 1. The fully developed slip-flow friction relation, fRe, is studied compared to the no-slip-flow case. The relation between the Knudsen number and the fRe is assumed in the form [30]

$$\mathrm{fRe}_{Kn} = \frac{1}{1 + CKn}\mathrm{fRe}_{Kn=0} \tag{21}$$

Rearranging the above equation in the form, $(\mathrm{fRe}_{Kn=0}/\mathrm{fRe}_{Kn} - 1) = CKn$, and plotting $(\mathrm{fRe}_{Kn=0}/\mathrm{fRe}_{Kn} - 1)$ against Kn as shown in Fig. 7a and observing the linear behavior, it can be concluded that the constant C is only a function of aspect ratio. Fig. 7b shows the variation of C with the channel aspect ratio. Correlation for the constant C is proposed from the least square fit with 0.999 coefficient of determination as

$$C = 11.93 - 11.32/\alpha + 10.32/\alpha^2 - 3.15/\alpha^3, \tag{22}$$

for the range of Kn and β considered.

4.4. Thermally developing temperature field

The effect of the Kn and β on the temperature profile is shown in Fig. 8 for thermally developing flow. It should be noted that the non-dimensionalized wall temperature is set equal to unity in all cases. As expected, for no-slip-flow ($Kn = 0$), no temperature jump is observed at the wall–fluid interface as shown in Fig. 8. As slip increases, the effect of Kn and β on the temperature profile becomes

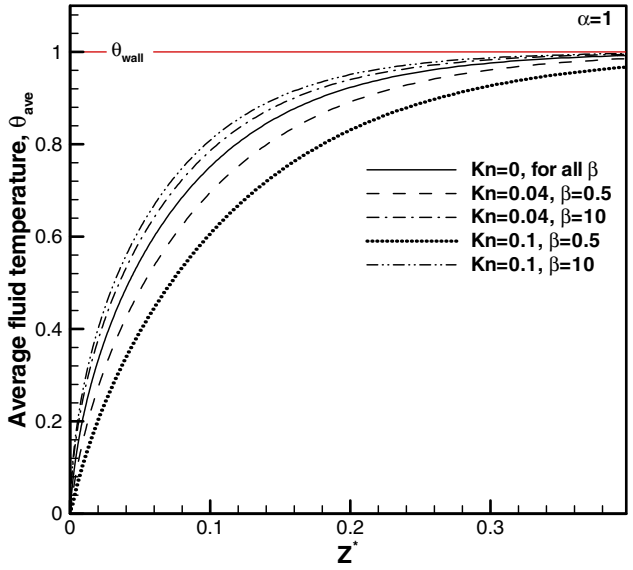

Fig. 9. Variation of average fluid temperature along the axis of a square microchannel for thermally developing flow at different Kn and β values.

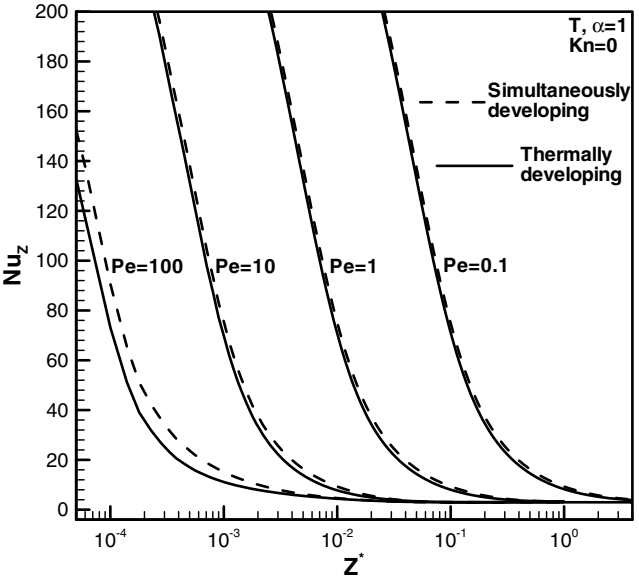

Fig. 10. Effect of Pe on developing local Nusselt number along the axis of a square microchannel for no-slip-flow case.

apparent. At low β values, the temperature profile deviates considerably from that of the no-slip-flow case due to large temperature jump that exits at the walls shown in Fig. 8a. As β increases, the temperature jump at the wall decreases and the temperature profile follows closely that of no-slip-flow case as shown in Fig. 8b. The average fluid temperature along the channel length, Z^*, is shown in Fig. 9 for thermally developing flow. As slip increases, the average fluid temperature can increase or decrease that of no-slip-flow case depending on the value of β. For low β values, the average fluid temperature is less than that of the no-slip-flow case and it increases as β increases and beyond a certain β, it reaches higher than that of no-slip-flow case as shown Fig. 9.

4.5. Nusselt number

The effect of *Pe* on the *Nu* number along the channel length for no-slip-flow (*Kn* = 0) is shown in Fig. 10 for a square channel under thermally and simultaneously developing flows. For low *Pe* values, a large increase of *Nu* is observed in the beginning of the entrance region as shown in Fig. 10. This is due to the strong axial conduction effects presence at low *Pe* values. For large *Pe* values, *Nu* reaches fully developed state at a much earlier stage and the difference between thermally and simultaneously developing *Nu* profiles become more obvious as shown in Fig. 10. Thus is due to the presence of strong advection effects at large *Pe* values.

In the case of slip-flow, the presence of the velocity slip and temperature jump can significantly affect the local *Nu* number. The velocity slip increases the advection near the walls causing an increase in the heat transfer whereas the temperature-jump increases the thermal resistance at wall–fluid interface resulting in a decrease in the heat transfer. Therefore, the combined effect of velocity slip and temperature jump could increase or decrease the heat transfer depending on their relative magnitude. Fig. 11a shows the effect of *Kn* and β on the developing *Nu* in the entrance region for *Pe* = 1. Here, slip-flow *Nu* number is compared to that of no slip-flow case. At the beginning of the entrance region, a drop in *Nu* is observed with the increase of *Kn* for all cases. This trend becomes more obvious at low β values as shown in Fig. 11a. This is due to the presence of large temperature jump at the beginning of the entrance region that results in a drop in *Nu*. Also it is interesting to observe that the *Nu* at the threshold of entrance is approaching a unique value, β/Kn, irrespective of the flow condition as predicted by Yu and Ameel [34]. As flow develops, at small β values, the effect of temperature jump remains dominant throughout the entrance region resulting in a decrease of *Nu* throughout the entrance length as shown in Fig. 11a for the case of *Kn* = 0.1 and β = 0.5. Beyond a certain value of β, velocity slip effect becomes more dominant over the temperature jump effect resulting in an increase of *Nu* as shown in Fig. 11b for the case of *Kn* = 0.1 and β = 10. Further, at low *Pe* values, there is not much difference between thermally and simultaneously developing *Nu* profiles are observed. As *Pe* increases, this difference becomes more apparent as shown in Fig. 11b.

Fig. 12 shows the fully developed *Nu* variation with *Kn* for different aspect ratios and β. When *Kn* = 0, the *Nu* is in good agreement with the results of Shah and London [33]. As *Kn* increases, *Nu* can increase, decrease or stay nearly constant depending on the value of β. Large reductions in *Nu* are observed at large aspect ratios as shown in Fig. 12. This could be due to the fact that the

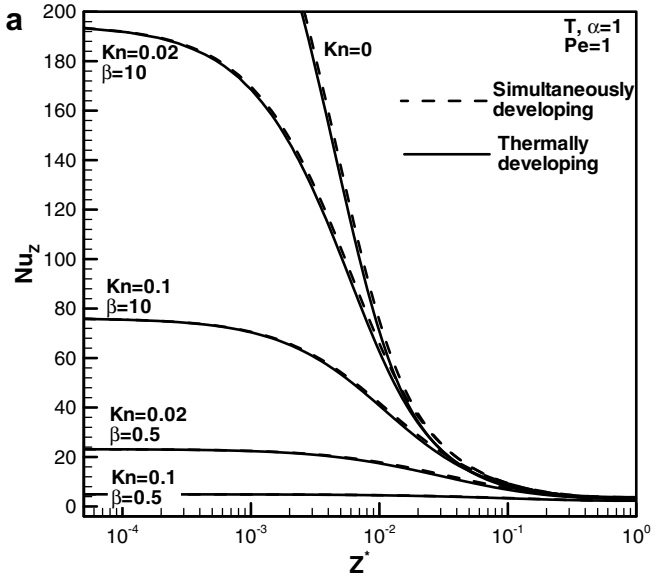

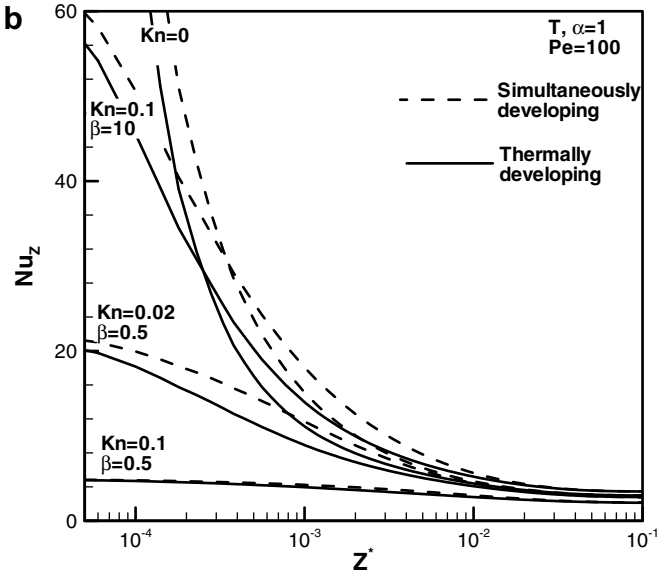

Fig. 11. Effect of *Kn* and β on the developing local Nusselt number along the axis of a square microchannel for (a) *Pe* = 1 and (b) *Pe* = 100.

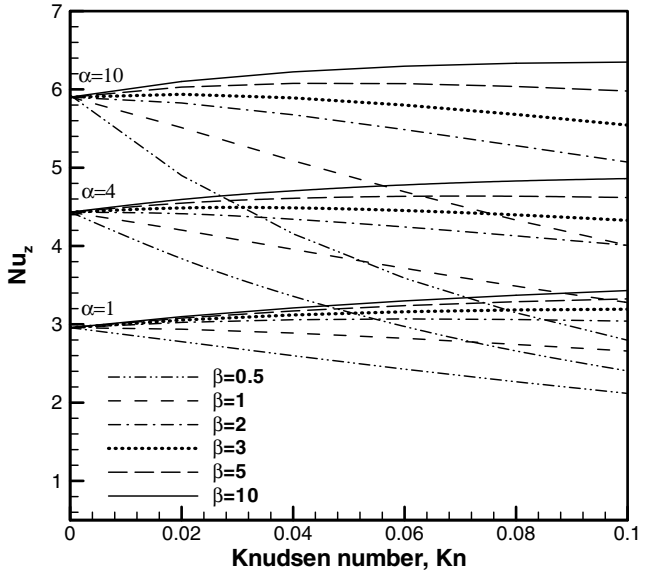

Fig. 12. Fully developed Nusselt number with the Knudsan number for different aspect ratios and β values.

temperature jump effect becomes more dominant over velocity slip effect at large aspect ratios. In the range of parameters considered, there could be high as a 15% increase or low as a 50% decrease in the fully developed *Nu* is possible due to slip-flow.

5. Conclusions

The effects of slip-flow on the flow field and heat transfer in rectangular microchannels with constant wall temperature walls has been studied numerically considering thermally and simultaneously developing flow conditions. Different channel aspect ratios ($1 \leqslant \alpha \leqslant 10$) were considered for Peclet numbers in the range of $0.1 \leqslant Pe \leqslant 100$ and Knudsen numbers in the range of $0 \leqslant Kn \leqslant 0.1$ with β in the range of $0.5 \leqslant \beta \leqslant 10$. The Navier–Stokes and energy equations are solved in a three-dimensional domain using the finite-volume method subjected to velocity slip and temperature jump boundary conditions. A modified convection–diffusion coefficient at the fluid–wall interface is defined to incorporate the temperature-jump boundary condition. The rarefaction effect decreases the velocity and pressure gradients in the channel resulting in a considerable reduction in the friction factor. The entrance length generally increases with the increase of *Kn* while the channels with aspect ratio near 4 are shown to have the largest entrance length. A correlation for the fully developed fRe is presented as a function of *Kn* and aspect ratio, α. The effect of *Pe*, *Kn* and β on Nusselt (*Nu*) number is investigated in the entrance region for thermally and simultaneously developing flows. The velocity slip has an increasing effect on the *Nu* number whereas temperature jump has a decreasing effect, and the combined effect could result in an increase or a decrease in the *Nu* number. The difference between simultaneously and thermally developing *Nu* numbers become more significant with the increase of *Pe* number. The fully developed *Nu* is determined for range of parameters. There could be high as a 15% increase or low as a 50% decrease in the fully developed *Nu* is possible due to slip-flow.

References

[1] E.G.R. Eckert, R.M. Drake Jr., Analysis of Heat and Mass Transfer, McGraw-Hill, New York, 1972. pp. 467–486.

[2] G. Karniadakis, A. Beskok, N. Aluru, Microflows and Nanoflows: Fundamental and Simulation, Springer, 2005.

[3] A. Beskok, G.E. Kamiadakis, Simulation of slip-flows in complex microgeometries, Micromech. Syst., ASME Proc. DSC 40 (1992) 355–370.

[4] E.B. Arkilic, K.S. Breuer, M.A. Schmidt, Gaseous flow in microchannels, Appl. Microfabr. Fluid Mech., ASME FED 197 (1994) 57–66.

[5] J.C. Harley, Y. Huand, H. Bau, J.N. Zemel, Gas flow in microchannels, J. Fluid Mech. 284 (1995) 257–274.

[6] E.B. Arkilic, M.A. Schmidt, K.S. Breuer, Gaseous slip flow in long microchannels, J. Microelectromech. Syst. 6 (2) (1997) 167–178.

[7] G.L. Morini, M. Spiga, Slip flow in rectangular microtubes, Microsc. Thermophys. Eng. 2 (1998) 273–282.

[8] A. Beskok, A model for flows in channels, pipes, and ducts at micro and nanoscales, Microsc. Thermophys. Eng. 3 (1999) 43–77.

[9] T. Araki, M.S. Kim, H. Iwai, K. Suzuki, An experimental investigation of gaseous flow characteristics in microchannels, Microsc. Thermophys. Eng. 6 (2002) 117–130.

[10] G.H. Tang, Z. Li, Y.L. He, W.Q. Tao, Experimental study of compressibility, roughness and rarefaction influences on microchannel flow, Int. J. Heat Mass Transf. 11–12 (50) (2007) 2282–2295.

[11] S.S. Hsieh, H.H. Tsai, C.Y. Lin, C.F. Huang, C.M. Chien, Gas flow in a long microchannel, Int. J. Heat Mass Transf. 47 (2004) 3877–3887.

[12] N. Dongari, A. Agrawal, A. Agrawal, Analytical solution of gaseous slip flow in long microchannels, Int. J. Heat Mass Transf. 50 (17-18) (2007) 3411–3421.

[13] H. Choi, D. Lee, J. Maeng, Computation of slip flow in microchannels using Langmuir slip condition, Numer. Heat Trans.; Part A: Appl. 1 (44) (2003) 59–71.

[14] O. Aydin, M. Avci, Thermally developing flow in microchannels, J. Thermophys. Heat Transf. 3 (20) (2006) 628–632.

[15] J.V. Rij, T. Harman, T. Ameel, The effect of creep flow on two-dimensional isoflux microchannels, Int. J. Therm. Sci. 11 (46) (2007) 1095–1103.

[16] L. Biswal, S.K. Som, S. Chakraborty, Effects of entrance region transport processes on free convection slip flow in vertical microchannels with isothermally heated walls, Int. J. Heat Mass Transf. 50 (7–8) (2007) 1248–1254.

[17] N.G. Hadjiconstantinou, O. Simek, Constant-wall-temperature Nusselt number in micro and nano-channels, J. Heat Transf. 124 (2002) 56–364.

[18] Z.P. Duan, Y.S. Muzychka, Slip flow in elliptic microchannels, Int. J. Therm. Sci. 11 (46) (2007) 1104–1111.

[19] R.F. Barron, X. Wang, T.A. Ameel, R.O. Warrington, The Graetz problem extended to slip-flow, Int. J. Heat Mass Transf. 40 (8) (1997) 1817–1823.

[20] T.A. Ameel, R.F. Barron, X. Wang, R.O. Warrington, Laminar forced convection in a circular tube with constant heat flux and slip flow, Microsc. Thermophys. Eng. 1 (4) (1977) 303–320.

[21] F.E. Larrodé, C. Housiadas, Y. Drossinos, Slip-flow heat transfer in circular tubes, Int. J. Heat Mass Transf. 43 (2000) 2669–2680.

[22] W. Sun, S. Kakac, A.G. Yazicioglu, A numerical study of single-phase convective heat transfer in microtubes for slip flow, Int. J. Therm. Sci. 50 (17) (2007) 3411–3421.

[23] M. Barkhordari, S.G. Etemad, Numerical study of slip flow heat transfer of non-Newtonian fluids in circular microchannels, Int. J. Heat Fluid Flow 5 (28) (2007) 1027–1033.

[24] S. Yu, T.A. Ameel, Slip flow heat transfer in rectangular microchannels, Int. J. Heat Mass Transf. 44 (2001) 4225–4234.

[25] S. Yu, T.A. Ameel, Slip-flow convection in isoflux rectangular microchannels, J. Heat Transf. 124 (2002) 346–355.

[26] M. Renksizbulut, H. Niazmand, G. Tercan, Slip-flow and heat transfer in rectangular microchannels with constant wall temperature, Int. J. Therm. Sci. 45 (9) (2006) 870–881.

[27] L. Kuddusi, Prediction of temperature distribution and Nusselt number in rectangular microchannels at wall slip condition for all versions of constant wall temperature, Int. J. Therm. Sci. 10 (46) (2007) 998–1010.

[28] L. Kuddusi, E. Cętegen, Prediction of temperature distribution and Nusselt number in rectangular microchannels at wall slip condition for all versions of constant heat flux, Int. J. Heat Fluid Flow 4 (28) (2007) 777–786.

[29] L. Ghodoossi, N. Egrican, Prediction of heat transfer characteristics in rectangular microchannels for slip flow regime and H1 boundary condition, Int. J. Therm. Sci. 6 (44) (2005) 513–520.

[30] W.A. Ebert, E.M. Sparrow, Slip flow in rectangular and annular ducts, J. Basic Eng., Trans. ASME (1965) 1018–1024.

[31] S.V. Patankar, Numerical Heat Transfer and Fluid Flow, Hemisphere, Washington, 1980.

[32] P. Wibulswas, Laminar Flow Heat Transfer in Noncircular Ducts, PhD thesis, London University, London, 1966.

[33] R.K. Shah, A.L. London, Laminar flow forced convection in ducts, Advances in Heat Transfer, Suppl. 1, Academic Press, New York, 1978.

[34] S. Yu, T.A. Ameel, A universal entrance Nusselt number for internal slip flow, Int. Commun. Heat Mass Transf. 28 (2000) 905–910.